In vivo bioluminescence tomography-guided system for pancreatic cancer radiotherapy research

Deng, Zijian; Xiangkun, X. U.; Dehghani, Hamid; Reyes, Juvenal; Zheng, Lei; Tran, Phuoc T.; Wang, Ken Kang Hsin

DOI:
10.1364/BOE.523916

Research Article Vol. 15, No. 8 / 1 Aug 2024 / Biomedical Optics Express 4525
Biomedical Optics EXPRESS

In vivo bioluminescence tomography-guided system for pancreatic cancer radiotherapy research

Zijian Deng,[1,2,3,7] Xiangkun Xu,[1,2] Hamid Dehghani,[4] Juvenal Reyes,[2] Lei Zheng,[5] Phuoc T. Tran,[6] and Ken Kang-Hsin Wang[1,2,8]

[1]*Biomedical Imaging and Radiation Technology Laboratory, Department of Radiation Oncology, University of Texas Southwestern Medical Center, Dallas, Texas 75390, USA*
[2]*Department of Radiation Oncology and Molecular Radiation Sciences, Johns Hopkins School of Medicine, Baltimore, Maryland 21231, USA*
[3]*Department of Biomedical Engineering, University of Texas Southwestern Medical Center, Dallas, Texas 75390, USA*
[4]*School of Computer Science, University of Birmingham, Birmingham B15 2TT, USA*
[5]*Sidney Kimmel Comprehensive Cancer Center, Department of Oncology, Johns Hopkins School of Medicine, Baltimore, Maryland 21231, USA*
[6]*Department of Radiation Oncology, University of Maryland School of Medicine, Baltimore, Maryland 21201, USA*
[7]*zijian.deng@utsouthwestern.edu*
[8]*kang-hsin.wang@utsouthwestern.edu*

Abstract: Recent development of radiotherapy (RT) has heightened the use of radiation in managing pancreatic cancer. Thus, there is a need to investigate pancreatic cancer in a pre-clinical setting to advance our understanding of the role of RT. Widely-used cone-beam CT (CBCT) imaging cannot provide sufficient soft tissue contrast to guide irradiation. The pancreas is also prone to motion. Large collimation is unavoidably used for irradiation, costing normal tissue toxicity. We innovated a bioluminescence tomography (BLT)-guided system to address these needs. We established an orthotopic pancreatic ductal adenocarcinoma (PDAC) mouse model to access BLT. Mice underwent multi-projection and multi-spectral bioluminescence imaging (BLI), followed by CBCT imaging in an animal irradiator for BLT reconstruction and radiation planning. With optimized absorption coefficients, BLT localized PDAC at 1.25 ± 0.19 mm accuracy. To account for BLT localization uncertainties, we expanded the BLT-reconstructed volume with margin to form planning target volume(PTV_{BLT}) for radiation planning, covering $98.7 \pm 2.2\%$ of PDAC. The BLT-guided conformal plan can cover 100% of tumors with limited normal tissue involvement across both inter-animal and inter-fraction cases, superior to the 2D BLI-guided conventional plan. BLT offers unique opportunities to localize PDAC for conformal irradiation, minimize normal tissue involvement, and support reproducibility in RT studies.

1. Introduction

Pancreatic cancer is the 7th leading cause of cancer death worldwide [1], and >90% of which is pancreatic ductal adenocarcinoma (PDAC) [2]. Present treatment approaches are ineffective, and novel strategies are desperately needed. The role of radiation therapy (RT) for pancreatic cancer has traditionally been assigned to palliation. The radio-immunotherapy, where high dose stereotactic body radiation therapy is used to elicit systemic treatment via immunotherapy agents, has stimulated excitement and inspired several clinical trials to treat pancreatic cancer [3–5]. The possibility of developing this treatment strategy has cast the use of radiation into a pivotal role in

#523916 https://doi.org/10.1364/BOE.523916
Journal © 2024 Received 15 Mar 2024; revised 19 May 2024; accepted 20 May 2024; published 9 Jul 2024

Biomedical Optics EXPRESS

the management of pancreatic cancer. Thus, there is a pressing need to investigate pancreatic cancer in pre-clinical setting to further advance our understanding of the role of RT.

Regarding important pre-clinical investigations of pancreatic cancer, the research setting needs to mimic the RT used for human. Such advanced technology is now available in the form of small animal irradiators [6,7], which are equipped with cone-beam computed tomography (CBCT) to guide radiosurgery-like delivery. While CBCT provides valuable irradiation guidance [8–11], it is less adept at localizing an abdominal malignancy growing in a low imaging contrast environment. Meanwhile, pancreatic tumor is prone to movement, leading to noticeable inter-fractional motion. With these targeting uncertainties, large radiation beams (e.g. 10 mm in diameter) are commonly used to irradiate pancreatic tumors [12,13] in animal model at the cost of normal tissue toxicity, leading to the concern of study reproducibility.

Because of the superior soft tissue contrast, non-ionizing features, and free of background noise, bioluminescence imaging (BLI) has been extensively applied in pre-clinical oncology studies [14–16], and it provides an attractive solution to localize pancreatic tumors for radiation studies [17,18]. However, because diffusive optical transport from an internal source to animal surface is highly susceptible to the irregular torso, tissue optical properties [19,20], and tumor movement, commercially available single-projection BLI system is inadequate in localizing abdominal targets for irradiation [17]. To address these challenges, we innovated volumetric bioluminescence tomography (BLT) to guide conformal irradiation for *in vivo* pancreatic tumors.

In tandem with a forward computational model of light propagation through tissue to the skin surface and an optimization algorithm, BLT can reconstruct the underlying 3D source distribution by minimizing the difference between calculated and measured surface BL signals [21–25]. Our BLT system is designed in standalone mode with a transportable bed that allows animal transport between the BLT system and irradiator [21,26]. To demonstrate our BLT system in localizing pancreatic malignancies for radiation guidance, we established a bioluminescent orthotopic PDAC model, which grows the tumor at single focus in pancreas to provide a well-controlled experimental environment. We inserted a titanium (Ti) wire at the center of tumor, which can be visualized in CBCT imaging used to inform tumor position and validate BLT target localization. PDAC-bearing mice were subject to multi-projection and multi-spectral BLI, maximizing the amount of measured data for accurate reconstruction [27–30], followed by CBCT imaging equipped in the irradiator for the generation of tetrahedral mesh used in BLT reconstruction and radiation planning. Longitudinal BL imaging was performed to demonstrate the inter-fractional tumor motion due to daily abdominal movement. To determine the optical absorption coefficients (μ_a) of mouse abdomen for accurate BLT target localization, we implanted an autoluminescent source into pancreas, and minimized the deviation of BLT localizing the source by tuning muscle-fat composition of abdomen that would affect the abdominal μ_a. We then illustrate the application of utilizing the BLT in monitoring the pancreatic tumor location in longitudinal manner. To demonstrate the capability of BLT in guiding irradiation for abdominal target, we used the mice bearing one-week PDAC for BLT-guided radiation planning. We use the location of Ti wire implanted within the center of the PDAC and the approximated tumor volume from the implanted tumor size to assess the BLT accuracy in both target localization and volume estimation. The margin for BLT-reconstructed target volume was designed, accounted for the BLT localization uncertainty, and applied in the planning process. We further compared the dosimetry between BLT-guided conformal plan and BLI-guided conventional anterior-posterior/posterior-anterior (AP/PA) plan to highlight the differences of tumor coverage and normal tissue involvement in both inter-animal and inter-fraction scenarios.

The significance of this work lies in its demonstration of BLT as an important image-guided modality for pre-clinical pancreatic cancer RT research. It enables precise localization of pancreatic malignancies *in vivo*, achieving conformal irradiation to minimize normal tissue toxicity, and therefore supporting study reproducibility.

Biomedical Optics EXPRESS

2. Materials and methods

2.1. Configuration of BLT system and small animal irradiator

We collaborated with our industrial partner and developed a BLT system, MuriGlo (Fig. 1(a)). The detail of the system is described in our previous study [26]. Briefly, the system is equipped with a rotatable 3-mirror assembly and a fixed mirror, directing bioluminescence emitted from the imaged object to a stationary charge-coupled device (CCD) camera. The 3-mirror system can rotate 360° around the object and capture images at multiple projection angles. The position where the 3-mirror is right above the mouse bed is labelled as 0°. The clockwise rotation is defined as positive direction, and the full range of rotation is defined from −180° to 180°. Optical filters installed ahead of the camera are used for multi-spectral image acquisition to improve BLT localization accuracy compared to single filter setting [27,28]. A thermostatic system is placed in the imaging chamber to maintain the mouse body temperature at 37 °C to keep consistent bioluminescence intensity throughout experiment and spectrum among animals, both of which are sensitive to ambient temperature [25]. A transportable mouse bed is used to hold the animal in both MuriGlo and small animal irradiator, and to support the animal transport between these two systems (Fig. 1(b)) [26].

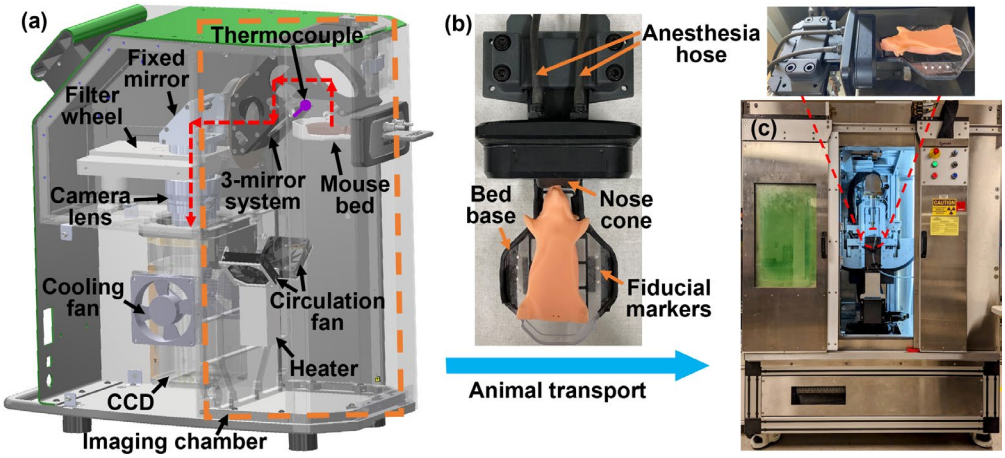

Fig. 1. illustrates the schematic of MuriGlo and the workflow of BLT-guided irradiation. (a) MuriGlo consists of an optical assembly, a thermostatic system, and a transportable mouse bed. The red dash line indicates the optical path from the imaging plane at the object through a 3-mirror system, a fixed mirror, a selected filter, and a camera lens to a CCD chip. The thermostatic system, including a heater, two circulation fans and a thermocouple at 3-mirror system, keeps the imaged object temperature at 37 °C to maintain stable intensity and consistent spectrum of bioluminescence emission throughout experiment. (b) The transportable mouse bed is composed of a bed base, a nose cone, eight fiducial markers and two anesthesia hoses. After optical image acquisition, the imaged animal is detached from MuriGlo along with the bed under anesthesia, and transferred to (c) a small animal irradiator for CBCT imaging and BLT reconstruction for BLT-guided irradiation.

Small animal radiation research platform (SARRP; Xstrahl Inc., Suwanee, GA) [6], a CBCT-equipped small animal irradiator, was used in this study for CBCT imaging and demonstrate BLI/BLT-guided radiation planning (Fig. 1(c)). SARRP uses a dual focal X-ray source for irradiation (220 kVp, 13 mA) and CBCT imaging (65 kVp, 0.7 mA). To achieve noncoplanar irradiation, it is equipped with a 360° isocentric gantry directing the X-ray source and a 4D robotic base (3-axis translation and 360° rotation) adjusting the loaded animal. For CBCT

Biomedical Optics EXPRESS

imaging, the animal was rotated with the bed between the X-ray source and an amorphous silicon flat panel detector. The acquired CBCT image was used to: 1) provide animal surface contour to generate the numerical mesh for BLT reconstruction, and 2) define 3D coordinate for radiation planning and irradiation.

2.2. In vivo orthotopic PDAC model

The details of the orthotopic PDAC model are described in Supplement 1 Sec. 1. Briefly, to establish this model using NCr nude mice (female, 6-8 weeks old; Taconic Biosciences, Rensselaer, NY), we injected 5×10^5 BxPC3-Red-FLuc cells (PerkinElmer, Waltham, MA) into the right flank of a mouse to grow a subcutaneous tumor. When the tumor reached around 10 mm in diameter, we harvested it, and then surgically implanted a fraction of the tumor, ~3 mm in diameter, into the pancreas of the targeted mouse. We also inserted a small piece of Ti wire (34 gauge, ~1 mm long; TEMCo Industrial, Fremont, CA) at the center of the implanted tumor as a fiducial marker to track the PDAC location, which can be visualized using the CBCT image.

2.3. Quantification of system-specific source spectrum

Because the spectrum weight of each wavelength data is considered equal in our reconstruction routine, it is necessary to quantify the spectral dependence of our BLIs before they can be used as the input data for the reconstruction [25]. The acquired BLIs include the overall spectral responses of the optical system and light source, and we named the resulted spectrum as system-specific source spectrum. Once the spectrum is known, the multi-spectral BLIs can be normalized to the quantified spectrum weighting, used as the input data for reconstruction.

We measured the system-specific spectral weights of the BxPC3-Red-Fluc cells at 590, 610, 630, and 650 nm in petri dishes with more than 80% confluency and D-Luciferin 0.75 mg/1 mL of phosphate buffer solution (PBS; pH 7.4, 1X) in place via MuriGlo controlled at 37 °C. A 10-μm-thick polyvinyl chloride membrane, transparent to the BLIs, was used to cover the petri dish to restrain vaporization that could take the heat away from PBS. The BLI acquisition was started 20 min after the dish was placed into the optical system to ensure the cells were heated and maintained at 37 °C. To eliminate the change of the *in vitro* spectral signal as a function of the luciferin incubation time, open-field (without filter) images were taken before and after each spectral BLI to quantify the *in vitro* signal variation over time. The time point for each image was recorded and open-field images were used to generate an *in vitro* time-resolved signal curve. We normalized the intensity of multi-spectral BLIs based on the time-variant data interpolated from the time-resolved curve. The spectral weights of the BxPC3-Red-Fluc at 590, 610, 630, and 650 nm and 37 °C are 0.6138 ± 0.0022, 1, 0.9247 ± 0.0019, and 0.5586 ± 0.0013 ($n = 5$), respectively.

2.4. In vivo Imaging protocol for BLI and BLT

We conducted the imaging session for three PDAC-bearing mice at 1, 1.5, 2, 3, and 5 weeks after tumor implantation. The imaging chamber was warmed up and maintained at 37 °C before the BLI course. The animal was anesthetized with 1-2% isoflurane in oxygen during the imaging session. Since orthotopic PDAC is closer to abdominal surface, the mice were immobilized in supine position during imaging to maximize the bioluminescence detection at 0° imaging projection. The mice were subject to multi-projection and multi-spectral BLI (8×8 binning, $4 \times$ pre-amplifier, 1 MHz readout rate) 10 minutes after intraperitoneal injection of D-Luciferin (125 μL, 30 mg/mL, PerkinElmer, Waltham, MA). We acquired images at the projections in the order of 0°, −90°, 180°, 90°. However, due to the location of orthotopic PDAC, minimum or no signal could be detected at 90° and 180° projections, so only the images at 0° and −90° projection were used for reconstruction. At each projection angle, four spectral images at 590, 610, 630, and 650 nm were acquired. The BLIs were corrected by the normalized spectral weights of

Biomedical Optics EXPRESS

BxPC3-Red-Fluc cells at the measured wavelengths. Open-field images were acquired before and after each spectral image to establish an *in vivo* time-resolved curve, which recorded signal variation over time to correct the intensity of each spectral image taken at a certain time point [25]. After BLI acquisition, photo images at −60°, −30°, 0°, 30°, and 60° were taken to record the positions of fiducial markers on the bed, which were also visible in CBCT image, to register the coordinates of MuriGlo and irradiator so we can map the BLI onto the numerical mesh surface of the animal generated from the SARRP CBCT image [26]. The data >10% of the maximum among all mapped surface data were used as the input for reconstruction. After the BLI acquisition, the animal along with the mouse bed was transferred from the optical system to irradiator for CBCT imaging.

We had also quantified the presence of any potential tumor movement or intra-fractional motion during the imaging session, involving optical and CBCT imaging at two close-by systems as well as the animal transport in between imaging (see Supplement 1 Sec. 2 for detail). Along with the aforementioned SARRP CBCT image captured after BLI, we also added additional CBCT imaging before the BLI, which involves an extra animal transport compared to a standard BLI-CBCT imaging session. In sum, we have animal well anesthetized and immobilized in the bed, and underwent SARRP-CBCT, MuriGlo-BLI and then SARRP-CBCT imaging. This process allowed us to visualize the position of Ti wire shown in both CBCT images, and quantify if there was PDAC displacement during the entire process. Despite the additional CBCT imaging and animal transport, the deviation of the Ti wire center between the two CBCT images was only 0.41 ± 0.11 mm (n = 9), indicating minimum target movement under our setup. This uncertainty was also propagated via the process of BLI mapped onto CBCT image, and thus to the BLT localization accuracy that was later considered in our BLT-guided radiation margin.

To eliminate the need of modeling light propagation from the animal surface to the camera in our non-contact imaging geometry, we applied a spectral derivative (SD) method and use the ratio of neighboring wavelength as the input data [31]. The reconstruction algorithm was previously published [25,32]. Due to the strong light scattering in tissue, diffusion equation was used to model light propagation in tissue media [33]. A reconstruction algorithm based on compressive sensing conjugate gradient optimization was chosen to retrieve BL tumor distribution [34]. Since the detected *in vivo* signal at 590 nm was much weaker than that at other wavelengths, which could introduce numerical errors with the SD method, we chose the images at 610, 630, and 650 nm for reconstruction. We used 50% of the maximum of reconstructed values as the threshold to delineate the BLT-reconstructed tumor.

2.5. Determination of optimal abdominal μ_a

BLT reconstruction is sensitive to μ_a, which changes greatly at our wavelength of interest. To ensure the accuracy of BLT localization, we proposed to determine the optimal μ_a of mouse abdomen for our animal cohort. We implanted a self-luminous light source (CBCT visible; 0.9 mm in diameter, 2 mm in length; Trigalight, mb-microtec ag, Niederwangen, Switzerland) into the pancreas of each mouse (n = 3). The spectral weights of three self-luminous sources, individually implanted into three mice, are listed in Supplement 1 Sec. 3 Table S1. The mouse abdomen was modeled as a mixture of muscle and fat [35]. Because the percentage of fat for 40 female mouse strains range from 16.7 ± 1.4% to 43.5 ± 1.3% [36], 46.1% was used as the maximum of fat composition at 95% confidence. Therefore, the maximum 46.1, average 22.9 [36] and 0% of fat were considered as the representatives to determine the range of μ_a. The approach of determining abdominal μ_a are described in Supplement 1 Sec. 4. The resulted μ_a at 610, 630, 650 nm are 0.1161, 0.0571, 0.0393 mm^{-1} for 0%, 0.0912, 0.0448, 0.0309 mm^{-1} for 22.9%, and 0.0658, 0.0324, 0.0224 mm^{-1} for 46.1% fat, respectively. The reduced scattering coefficients (μ_s') at 610, 630, 650 nm exhibit relative constant behavior, and thus we used published values, 1.4635, 1.4041, 1.3487 mm^{-1}, for the mice abdomen region [37]. The refractive index was

Biomedical Optics EXPRESS

set as 1.4 [38]. The deviation between the center of mass (CoM) of BLT-reconstructed light source and the known source center was calculated corresponding to the range of μ_a we chose and the optimal μ_a was adopted for the BLT-guided planning. The deviations contributed from different μ_a sets is considered statistical difference when $P < 0.05$, calculated by a two-tailed paired Student's t-test (Microsoft 365 Excel; Microsoft, Redmond, WA).

2.6. In vivo BLT- and BLI-guided radiation planning

The gross target volume (GTV) of the PDAC is needed to quantify the localization uncertainty of the BLT-reconstructed volume (GTV_{BLT}) and to assess the dosimetry coverage. Since the implanted PDAC likely underwent angiogenesis at early stage, we hypothesized that it would not grow significantly at 1 week after implantation. Therefore, we used the 1st-week PDAC to define approximated GTV (aGTV), estimated with the implanted tumor size located at the Ti wire, for BLT-guided radiation planning. A radiation margin accounting for the uncertainties of BLT guidance was added to GTV_{BLT} to form a BLT planning target volume (PTV_{BLT}). The margin size is determined by maximizing GTV coverage while minimizing normal tissue involvement. The PTV_{BLT} coverages on GTV and abdominal tissue were defined as $(PTV_{BLT} \cap GTV)/GTV$ and $[PTV_{BLT} - (PTV_{BLT} \cap GTV)]/V_{abdomen}$, respectively, where $V_{abdomen}$ is the abdomen volume. We designed 6-arc conformal BLT-guided radiation plan using motorized variable collimator (MVC) and SARRP treatment planning system, MuriPlan (version 3.0.0; Xstrahl Inc., Suwanee, GA). The arc isocenter was set at GTV_{BLT} CoM with the goal of 5 Gy prescribed dose covering 95% of PTV_{BLT}.

To mimic the best image-guided irradiation possibly achieved by BLI system, we devised a BLI-guided conventional AP/PA plan with 10×10 mm^2 field, a field size commonly used for pancreatic tumor irradiation [12,17,18]. The centers of the AP/PA beams were positioned through the BLI maximum point along the AP direction obtained from a single-projection image. The beam isocenter was set at the midline of mouse body to achieve a uniform dose volume covered by the 5 Gy prescribed dose. The BLI AP/PA plan was compared with the BLT-guided conformal plan to investigate the differences of BLI and BLT guidance in abdominal tumor coverage and normal tissue involvement in both inter-animal and inter-fraction cases.

3. Results

3.1. Inter-fractional tumor motion

Figure 2 shows BLI and CBCT images acquired at 1.5 (Fig. 2(a)) and 3 (Fig. 2(b)) weeks after tumor implantation from the same animal. We utilized the first open-field images, captured 10 minutes after luciferin injection, as the representative BLIs, which is less susceptible to signal variation *in vivo*. The BLIs were also normalized with imaging acquisition time. As depicted in Fig. 2(a1) and b1, due to the inter-fractional motion of PDAC, the BL signal appeared at different locations on abdominal surface, shown in the two imaging sessions. In contrast to the typical increase in bioluminescence intensity with tumor growth, the BL signal was notably reduced at 0° projection (Fig. 2(a1) vs. b1), while we noticed the signal increase at 180° projection (Fig. 2(a2) vs b2). This phenomenon could be attributed to the inter-fractional motion, validated in CBCT images (Fig. 2(a3) and b3). The mobility of abdominal tumor introduced the challenges in tumor localization and growth monitoring using single-projection 2D BLI. It emphasizes the need of volumetric BLT as the image-guidance for abdominal tumor irradiation.

3.2. Optimal abdominal μ_a for BLT reconstruction

To obtain the optimal abdominal μ_a, 3 sets of μ_a with 0, 22.9 and 46.1% fat composition (Table 1) were applied to the BLT reconstruction in determining the CoM position of the light source implanted in mice (n = 3). Figure 3 shows the BLT-reconstructed CoM deviate the most from the

Biomedical Optics EXPRESS

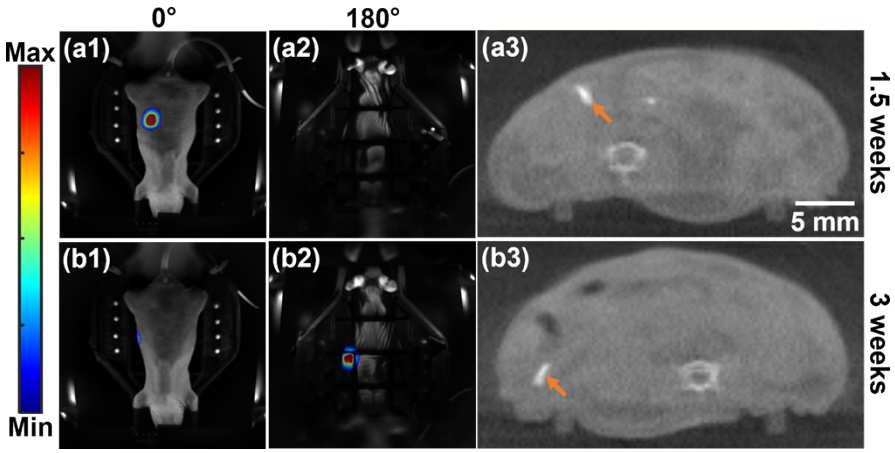

Fig. 2. shows the first open-field BLI (a) 1.5 and (b) 3 weeks after tumor implantation at (a1 and b1) 0 and (a2 and b2) 180° projections with corresponding SARRP CBCT images (a3 and b3).

true source location, when the μ_a derived from the 46.1% fat composition was chosen. Table 1 presents the overall results of the deviation between the BLT-reconstructed CoM and the actual center of source for all three mice for a given set of μ_a. The deviation became larger as the fat composition increased, and the deviation of the 46.1% group was found to be significantly different ($P < 0.05$) from that of 0 and 22.9% group. The optimal range of fat composition for our animal cohort could be 0-22.9%. The set of μ_a with 0% fat composition were utilized as the optimal values applied in the BLT reconstruction for the orthotopic PDAC model.

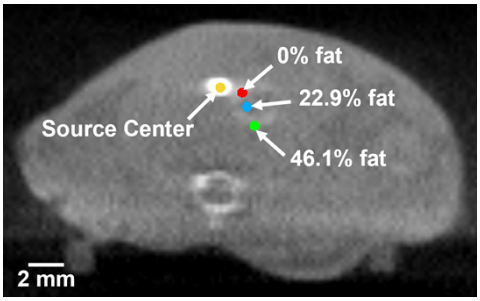

Fig. 3. The deviation between actual center of autoluminescent source implanted in pancreas and CoM of BLT-reconstructed source distribution corresponding to spectral-dependent μ_a (Table 1) is shown; three CoMs were projected at the same transverse slice in the CBCT image to visualize their deviations from the actual source.

Table 1. Deviations between CoM of BLT-reconstructed source distribution and center of CBCT-imaged autoluminescent source with set of μ_a as function of fat composition.

Fat %	0%			22.9%			46.1%		
Wavelength (nm)	610	630	650	610	630	650	610	630	650
μ_a (mm^{-1})	0.1161	0.0571	0.0393	0.0912	0.0448	0.0309	0.0658	0.0324	0.0224
Deviation (mm)	1.03 ± 0.60			1.15 ± 0.85			2.08 ± 1.01		

Biomedical Optics EXPRESS

3.3. *In vivo BLT*

Figure 4(a-c) show an example of BLT reconstruction for the orthotopic PDAC model. The acquired BLIs were mapped onto the surface of tetrahedral mesh generated from the mouse CBCT image (Fig. 4(a)). The GTV_{BLT} was overlapped with aGTV in both transverse cross-section of CBCT image (Fig. 4(b)) and 3D rendering (Fig. 4(c)). The deviation between CoM of BLT reconstruction and Ti wire center was 0.96 mm. In Fig. 4(d), we detailed the accuracies of BLT localization for all three mice at 1 1.5, 2, 3, and 5 weeks after tumor implantation, which were in the range of 0.5-2 mm, indicating no significant correlation between the accuracy of BLT localization and the tumor age. Our BLT system retrieved the orthotopic PDAC at depth of 2-6 mm from abdominal surface with the accuracy of 1.25 ± 0.19 mm ($n = 15$ for all the image sessions). In addition to the localization accuracy, we also assessed the volume and integrated bioluminescent power retrieved from BLT reconstruction, which are related to the tumor growth and viability, for these imaged mice at various time points (Supplement 1 Sec. 5 for detail). Figure S3 shows an increasing trend in reconstructed volume and integrated power as the tumor grew.

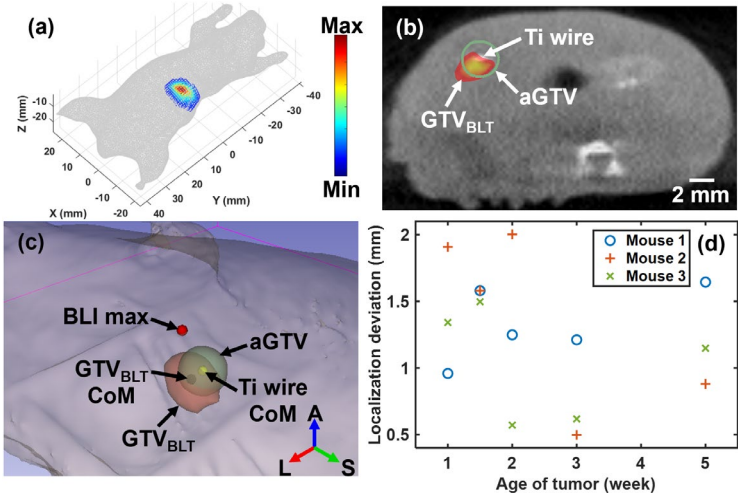

Fig. 4. BLT reconstruction for the mice bearing orthotopic PDAC; (a) the 0° and -90° projection BLIs at 630 nm mapped onto mesh surface after correcting time-resolved signal variations and source spectrum; data > 10% of maximum within these two projections were mapped and used for reconstruction. (b) Transverse view of CBCT image and (c) 3D rendering overlapped with aGTV (green contour) and GTV_{BLT} (heat map in b and red contour in c) with 50% threshold; center of Ti wire (yellow dot), CoM of GTV_{BLT} (black dot) and maximum point of BLI shown at 0° projection (red dot) were marked on animal surface. (d) shows the deviations between center of Ti wire and CoM of GTV_{BLT} for the three mice at 1, 1.5, 2, 3, and 5 weeks after tumor implantation.

3.4. *BLT- vs. BLI-guided radiation planning*

Figure 5 demonstrates the superior capability of BLT for guiding irradiation in orthotopic PDAC when compared to BLI-guidance, especially in terms of tumor coverage and reduced radiation toxicity to normal tissue. The mice in Fig. 5 were numbered according to Fig. 4(d). In Fig. 5(a) and b, we present the radiation planning for two PDAC-bearing mice (Mouse #1 and #3, respectively) at 1 week after tumor implantation. Due to the inter-fractional motion, although the tumors of different mice were implanted at the same location on the same day, their BLI

Biomedical Optics EXPRESS

patterns appeared at different places on abdomen surface (Fig. 5(a1-2) and b1-2, mice at supine position) during imaging session. Moreover, since the tumor of Mouse #3 had shifted to the left flank (Fig. 5(b1-2)), where a high surface gradient was present, the BLI at 0° projection was insufficient to even approximate tumor location. Therefore, the use of multi-projection BLIs were crucial to capture sufficient surface BL information to achieve accurate BLT reconstruction for the abdominal target.

Although the GTV_{BLT} could localize the tumor (Fig. 5(a3-4) and b3-4), the accuracies of its positioning and volume delineation were inevitably affected by multiple light scattering in tissue, the tomographic reconstruction under ill-posed condition, and uncertainties in optical property determination. To compensate the BLT localization uncertainties and ensure sufficient dose coverage of aGTV, we added a uniform margin on GTV_{BLT} to form a PTV_{BLT} for radiation guidance. With a 1.5 mm margin expansion, the PTV_{BLT} could cover $98.7 \pm 2.2\%$ ($n = 3$) of aGTV at 1 week after tumor implantation. Further increasing margin could involve more normal tissue in PTV_{BLT} without significant improvement of tumor coverage. We designed MVC-based noncoplanar 6-arc plan, with arc isocenter positioned at GTV_{BLT} CoM, optimized for the PTV_{BLT} coverage of each mouse (Supplement 1 Sec. 6, Table S4). The dose distributions of Mouse #1 and 3, with prescribed dose of 5 Gy to cover 95% of PTV_{BLT}, demonstrated that our BLT-guided conformal irradiation can fully cover the aGTV while restraining normal tissue involvement, regardless of tumor location (Fig. 5(a3-4) and b3-4). The corresponding BLI-guided irradiation plans are shown in Fig. 5(a5-6) and b5-6 for comparison. The AP/PA arrangement with 10×10 mm^2 field was applied. We positioned the isocenter at the midline along the BLI maximum point at 0° projection image, and set 5 Gy cover the irradiated volume. To compare the accuracy of beam targeting in these two plans, we projected the BLI maximum and GTV_{BLT} CoM onto the X-Y plane where the Ti wire center was located. For Mouse #1, despite the spatial deviation of the projected BLI maximum compared to GTV_{BLT} CoM (Fig. 5(a6)), the large AP/PA field could still fully cover the aGTV (Fig. 5(a5-6)). However, for Mouse #3, as the tumor was located at the left flank, the projected BLI maximum point was farther away from the source (Fig. 5(b6)). Consequently, the aGTV could not be effectively covered by the 5 Gy iso doseline (Fig. 5(b5-6)). Furthermore, because of the BLI maximum point located close to the left side of mouse, part of AP/PA field was positioned outside the animal body, leading to the quite inconsistent irradiated volume compared to mouse # 1 (Fig. 5(a5-6) vs. b5-6).

To demonstrate the capability of BLT in guiding irradiation for targets involving inter-fraction motion, we compare BLT-guided conformal and BLI-guided conventional AP/PA plans for an PDAC-bearing mouse at two different imaging sessions conducted at 1 (Fig. 5(b)) and 1.5 (Fig. 5(c)) weeks after tumor implantation, respectively. The inter-fraction movement of PDAC was noticeable in BLI (Fig. 5(b1-2) vs. c1-2), and CBCT images (Fig. 5(b3-6) vs. c3-6). Despite the motion, our BLT-derived PTV_{BLT} can completely covered the aGTV with minimal involvement of normal tissue, allowing the 6-arc conformal irradiation (Fig. 5(b3-4) vs. c3-4). In contrast, for the BLI-guided AP/PA plan, in addition to the inconsistent irradiated volume, the spinal cord was unfavorable included in the beam path at the 1.5-week case (Fig. 5(b5-6) vs. c5-6). The radiation to spinal cord could potentially introduce paresis. The variations in normal tissue irradiation ultimately introduce study uncertainties.

Figure 6 shows the corresponding dose-volume histograms (DVH) of the plans described in Fig. 5. The blue solid curves are the PTV_{BLT} DVH curves with 5 Gy prescribed dose covering 95% of the PTV volume. The BLT-guided conformal plans achieved 100% coverage of aGTV at the prescribed dose (red solid curve). In contrast, despite the large irradiation volume, the AP/PA plan cannot fully cover the aGTV with the prescribed dose (Fig. 6(b), red dash curve, 96.4% coverage). In terms of normal tissue involvement, only 1.6, 1.5 and 1.2% of normal tissue were at 5 Gy in the BLT-guided plans (green solid curves, Fig. 6(a-c)), which was distinctly less than 13.0, 5.4 and 11.2% in the BLI-guided plans, respectively (green dash curves). It is worthwhile

Biomedical Optics EXPRESS

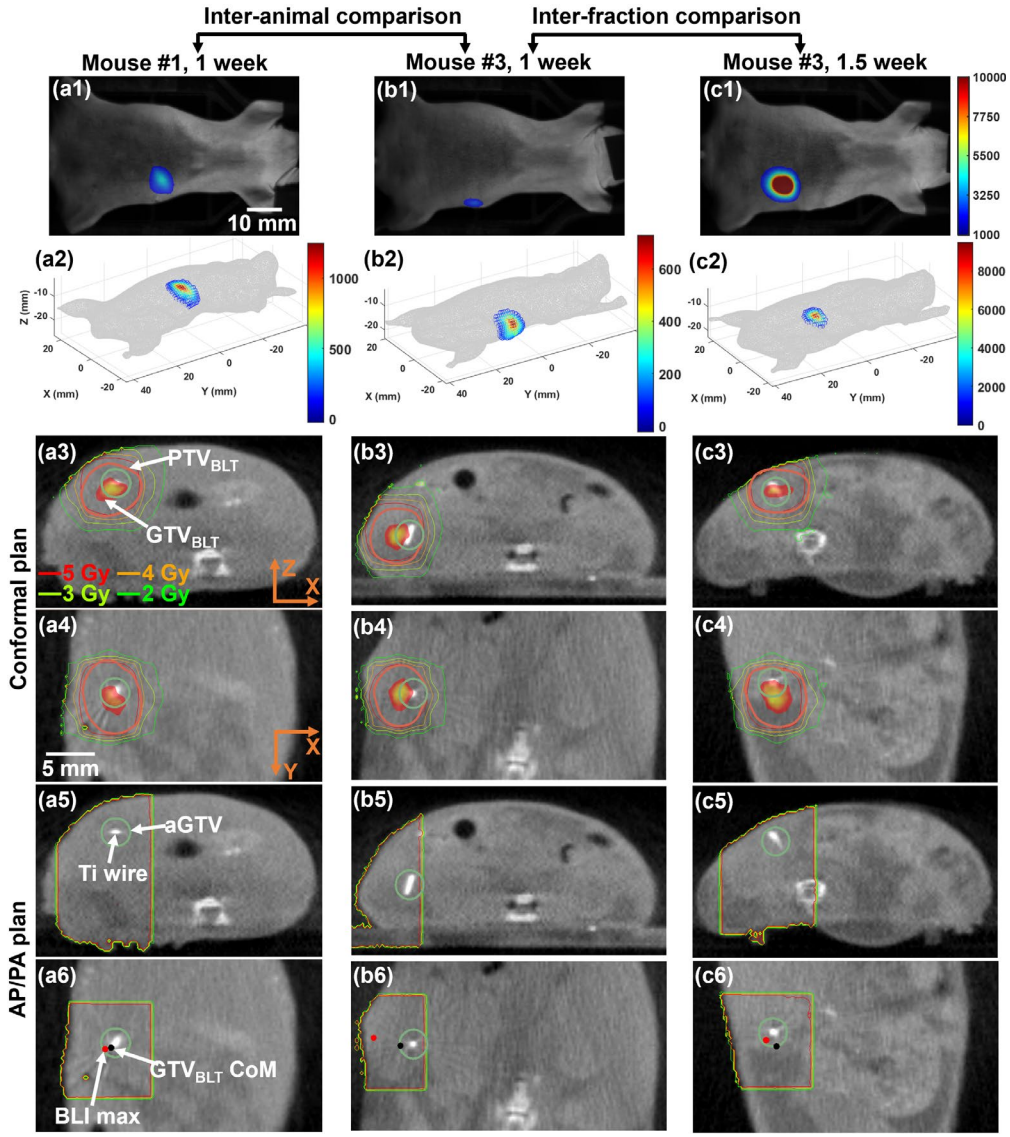

Fig. 5. BLT-guided 6-arc conformal plan vs. BLI-guided conventional AP/PA plans for inter-animal comparison between Mouse (a) #1 and (b) #3 at 1 week after tumor implantation, and for inter-fraction comparison of Mouse #3 at (b) 1 and (c) 1.5 weeks after tumor implantation; for each data set (Fig. a, b, or c): (a-c1) show 0° projection BLI at 630 nm; (a-c2) are 0° and 90° projection BLIs at 630 nm mapped onto mesh surface; data > 10% of maximum (10% threshold) within these two projections were displayed. Transverse and coronal views of CBCT image overlapped with aGTV (green contour), GTV_{BLT} (50% threshold, heat map), PTV_{BLT} (red contour), and isodose distributions of BLT-guided conformal and BLI-guided AP/PA plans are shown in Fig. (a-c3 and a-c4) and (a-c5 and a-c6), respectively. GTV_{BLT} CoM (black dot) and BLI maximum point (red dot) were projected onto the coronal view where the center of Ti wire was located, Fig. (a-c6).

Biomedical Optics EXPRESS

to mention that consistent with the results of Fig. 5, the 5.4% normal tissue volume covered by 5 Gy is inconsistent compared to that of mouse 1 or even the same mouse at different imaging time point, indicating the deficiency of BLI-guided plan for motion targets. The high conformality of PTV_{BLT} coverage shown in the BLT-guided plans effectively constrained the dose around the aGTV. Spanning the wide dose range from 2-5 Gy, the BLT-guided plans showed less normal tissue involvement (green solid vs dash curves).

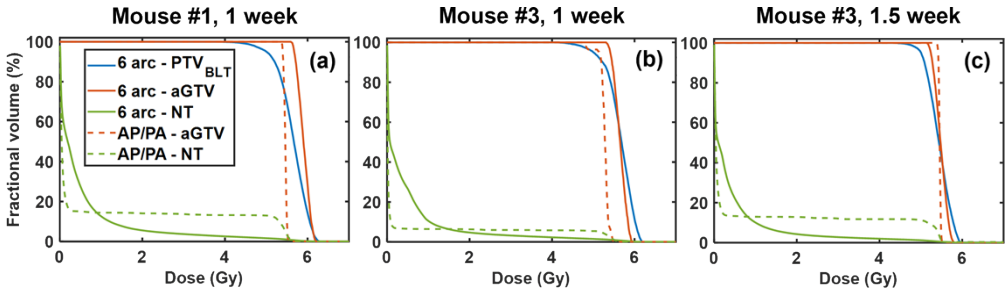

Fig. 6. The corresponding DVHs of BLT-guided 6-arc and BLI-guided AP/PA plans for the three data sets described in Fig. 5. The PTV_{BLT} DVH is only for the BLT-guided plan and the aGTV and normal tissue (NT) DVHs are for both plans.

4. Discussion

Current treatments for pancreatic cancer are lacking effectiveness, prompting a shift towards innovative strategies. Radio-immunotherapy has attracted significant interest for its potential to treat pancreatic cancer [3–5]. The evolving role of radiation therapy in managing pancreatic cancer emphasizes further research in pre-clinical settings to advance our understanding of the role of radiation. The orthotopic pancreatic tumor model is favored for radiobiology studies because tumors that develop in the microenvironment of the originating organ provide a more realistic representation of human pancreatic cancer than ectopic models. To align pre-clinical research with clinical practice, CBCT-equipped small animal irradiators have been developed to enable precise radiation delivery to animal models [6,7]. However, CBCT is limited in localizing soft tissue targets in a low contrast tissue environment. This limitation becomes more pronounced when using CBCT to guide irradiation for orthotopic PDAC, where both the tumor and pancreas are subject to motion (Fig. 2), leading to significant inter-fractional displacement. This could lead to a major concern for fractionation study as different volume of normal tissue or organ at risk (OAR) exposed to irradiation. As a result, CBCT-guided irradiation often requires planning with a large field to ensure tumor coverage at the cost of increased normal tissue toxicity [12,13], ultimately affecting the reproducibility of studies. Recognizing that CBCT imaging is inadequate to guide the irradiation for *in vivo* pancreatic tumor, we identified the powerful solution of incorporating molecular 3D BLT as an innovative image-guided system.

Before investigating the BLT-guided studies for the *in vivo* PDAC, we also quantified any significant tumor movement during imaging-guided sessions, i.e., intra-fractional motion (see Supplement 1 Sec. 2 for detail). Ensuring that the animals were well anesthetized and immobilized on the bed, and with the irradiator and optical system in close proximity, we managed to maintain minimal intra-fraction PDAC movement of 0.41 ± 0.11 mm ($n = 9$) during the imaging sessions significantly less compared to the inter-fractional motion (Fig. 5(b1) vs c1 and b3 vs c3). Additionally, this intra-fractional localization uncertainty was propagated during the process of mapping BLI onto the CBCT image because a displaced bioluminescent tumor would influence the surface pattern of BLI. Thus, this uncertainty could subsequently affect BLT target localization accuracy, which we considered in our BLT-guided radiation margin.

Biomedical Optics EXPRESS

Optical properties, particularly μ_a, could affect the accuracy of BLT reconstruction [39]. To retrieve the optimal μ_a for mouse abdominal tissue, we derived the μ_a by examining different composition of muscle and fat [35,36] in affecting BLT target localization accuracy. Because muscle and fat are the major components of abdominal tissue, and high absorption organs, e.g., liver and kidney, were absent in close proximity to the PDAC in our study cohort, the two-component muscle-fat model is sufficient to estimate the abdominal μ_a. The optimal values of the spectrally resolved μ_a were determined with fat ranging from 0-22.9% which allows the best localization accuracy in abdominal region (Fig. 3 and Table 1). With the optimized optical property, our BLT system can achieve 1.25 ± 0.19 mm, irrespective of the PDAC growth (Fig. 4(d)). Beyond its superiority in target positioning, BLT can also potentially quantify both tumor volume and emitted bioluminescent power of tumors (Fig. S3). As the bioluminescence represents cell viability, the BLT reconstructed tumor volume and emitted power could be valuable metrics for tumor growth monitoring and treatment response assessment. To further improve the determination of μ_a, we are implementing simultaneous diffuse optical tomography and BLT algorithm to adaptively retrieve optical properties for a given animal, within the BLT framework during the iterative source reconstruction process [40,41]. This algorithm will be integrated with our BLT system to advance image-guided RT.

The surface BLI has been adopted to guide irradiation for orthotopic PDAC model [17,18]. However, in addition to tissue absorption and scattering affecting light transport [19,20], the light diffused from bioluminescent tumor to animal surface is also highly susceptible to the surface gradient, which varies with the tumor location (Fig. 5). This makes it challenging to employ commonly-used single-projection BLI for guiding irradiation to the PDAC at high accuracy; Tuli et al. had to used 4 mm radial margin with collimator size in 10-15 mm diameter to irradiate the orthotopic pancreatic tumor based on 2D BLI [17]. Rapic et al. further advanced the BLI-guidance through multi-projection and -spectral images, and used an analytical model to calculate the internal source position [18]. This model assumed the BL source is a single point at the center of tumor. Their results are encouraging as it shows the depth difference between the optical source and actual pancreatic tumor is around -0.5 mm, where BLI-retrieved optical source was at deeper depth, ranging from 1.29 to -2.35 mm at 95% confidence interval. However, the 3D deviation of the BLI target localization accuracy for the orthoptic pancreatic tumor was not reported, which is challenging to justify the BLI targeting accuracy. Because a single point source was assumed in the model which does not allow for 3D tomography of the BL signal, the BLI-guided method is not able to provide 3D information pertinent to conformal irradiation, i.e., tumor volume and shape.

In this work, we further compare the BLI-guided conventional plan vs. BLT-guided conformal plan for the orthotopic pancreatic tumor irradiation especially in the situation where tumor displacements between animals and fractions are involved. Although BLI-guided plan is relatively simple, based solely on the location of surface BLI maximum, large collimation is unavoidably used to ensure conservative radiation coverage, mitigating the risk of missing the target. While tumor coverage may be achievable, BLI-guided irradiation inevitably involves a considerable portion of normal tissue, elevating the risk of radiation damage to critical organs (i.e., spinal cord shown in Fig. 5(c5-6)). Irradiating spinal cord can lead to paresis. This, in turn, amplifies experimental uncertainty and diminishes reproducibility of radiobiological discoveries, when inconsistent normal tissue is irradiated. Furthermore, the volume of involved normal tissue varied significantly with the specific location of PDAC (Fig. 5 and 6). This variability induces not only different levels of damage to normal tissue among mice within the same experimental group, but also for the same mouse treated at different radiation fraction. Fractionation is commonly employed in clinical RT, enabling self-repair of healthy cells during rest periods to reduce radiation toxicity in normal tissue, and it has been a common RT study scenarios in several pre-clinical investigations [42–45]. Our results demonstrate that BLI-guided irradiation can vary

Biomedical Optics EXPRESS

the volume of normal tissue covered at different fractions for orthotopic PDAC RT study, which would underdetermine or overestimate the efficacy of applying fractionation scheme for normal tissue repair in response to irradiation.

Our BLT-guided irradiation represents a significant advancement beyond BLI-guided irradiation especially for the orthotopic pancreatic tumor RT study, demonstrated in Fig. 5. In tandem with the model of light propagation through tissue to surface and the optimization algorithm, we have transitioned from the surface-guided irradiation to the volumetric-guided scheme. This leap is a substantial step toward mimicking the clinical scenario in which we can tailor conformal irradiation to the retrieved distribution of orthotopic PDAC. To accommodate the uncertainty of BLT localization, we designed the radiation margin for the BLT-reconstructed volume, maximizing target coverage with minimum involvement of normal tissue. With the volumetric information and high accuracy of target localization, we can effectively design the BLT-guided margin as small as 1.5 mm and irradiation field size between 6×6 and 7×7 mm^2 (Supplemental material Sec. 5). Despite the significant tighter margin and smaller field size are used, compared to other [17,18] and our BLI-guided plan (Fig. 5(a5-6), b5-6, c5-6) (2-4 mm margin, 10-15 diameter or 10×10 mm^2 field size), the BLT-guided conformal irradiation can achieve sufficient tumor coverage at prescribed dose while effectively restraining and minimize the involvement of normal tissue around the target (Fig. 5 and 6). Our results further demonstrated that BLT-guided system could successfully guide irradiation for the orthoptic pancreatic tumor even it is susceptible for abdominal movement (Fig. 5(a3-4), b3-4, c3-4). The reduction of radiation toxicity on normal tissue, especially critical organs, facilitates the robustness of experimental conclusions, thus ensuring our BLT-guided radiation platform to be reliable for multi-animal and fractionated RT research for pancreatic cancer.

5. Conclusion

Pancreatic cancer remains a major global health challenge, as existing treatments showing limited efficacy. The growing interest in radio-immunotherapy has highlighted radiation's central role in managing pancreatic cancer. Accurate localization of pancreatic tumors during radiation is crucial to irradiate them effectively and to reduce radiation toxicity to adjacent healthy tissues. Traditional CBCT-guided systems have shown shortcomings in localizing these tumors, particularly in motion-sensitive abdominal areas. The introduction of BLT offers a promising solution to these challenges, providing superior soft tissue contrast and effective localization of pancreatic malignancies *in vivo*. We have pioneered an *in vivo* BLT-guided system for pancreatic cancer, enabling highly conformal irradiation, previously unachieved for the orthotopic pancreatic tumor model. This advancement minimizes radiation-induced damage to normal tissues and ensures more consistent study outcomes. Our work underscores the potential of BLT as an invaluable imaging modality to allow clinically similar irradiation in the orthotopic pancreatic tumor, bridging the gap between pre-clinical research and clinic translational study for pancreatic cancer.

Funding. Cancer Prevention and Research Institute of Texas (RR200042); National Cancer Institute (P30CA006973, R01CA240811, R21CA223403, R37CA230341).

Disclosures. The research group of Dr. Ken Kang-Hsin Wang and Xstrahl are supported by NIH academic-industrial partnership R37CA230341 in the development of BLT-guided system for pre-clinical radiation research.

Data availability. Data underlying the results presented in this paper are not publicly available at this time but may be obtained from the authors upon reasonable request.

Supplemental document. See Supplement 1 for supporting content.

References

1. H. Sung, J. Ferlay, R. L. Siegel, *et al.*, "Global cancer statistics 2020: Globocan estimates of incidence and mortality worldwide for 36 cancers in 185 countries," Ca-Cancer J. Clin. **71**(3), 209–249 (2021).

Biomedical Optics EXPRESS

2. M. Orth, P. Metzger, S. Gerum, *et al.*, "Pancreatic ductal adenocarcinoma: Biological hallmarks, current status, and future perspectives of combined modality treatment approaches," Radiat. Oncol. **14**(1), 141 (2019).
3. . "Chemoimmunotherapy and radiation in pancreatic cancer (CRIT)," (ClinicalTrials.gov.).
4. . "Pancreatic tumor cell vaccine (GVAX), low dose cyclophosphamide, fractionated stereotactic body radiation therapy (SBRT), and folfirinox chemotherapy in patients with resected adenocarcinoma of the pancreas," (ClinicalTrials.gov.).
5. . "Immune checkpoint inhibition (Tremelimumab and/or MEDI4736) in combination with radiation therapy in patients with unresectable pancreatic cancer," (ClinicalTrials.gov.).
6. J. Wong, E. Armour, P. Kazanzides, *et al.*, "High-resolution, small animal radiation research platform with X-ray tomographic guidance capabilities," Int. J. Radiat. Oncol., Biol., Phys. **71**(5), 1591–1599 (2008).
7. M. Matinfar, E. Ford, I. Iordachita, *et al.*, "Image-guided small animal radiation research platform: Calibration of treatment beam alignment," Phys. Med. Biol. **54**(4), 891–905 (2009).
8. G. S. Herter-Sprie, H. Korideck, C. L. Christensen, *et al.*, "Image-guided radiotherapy platform using single nodule conditional lung cancer mouse models," Nat. Commun. **5**(1), 5870 (2014).
9. A. Chandra, T. Lin, M. B. Tribble, *et al.*, "PTH1-34 alleviates radiotherapy-induced local bone loss by improving osteoblast and osteocyte survival," Bone **67**, 33–40 (2014).
10. L. Seifert, G. Werba, S. Tiwari, *et al.*, "Radiation therapy induces macrophages to suppress T-cell responses against pancreatic tumors in mice," Gastroenterology **150**(7), 1659–1672.e5 (2016).
11. W. Sievert, S. Stangl, K. Steiger, *et al.*, "Improved overall survival of mice by reducing lung side effects after high-precision heart irradiation using a small animal radiation research platform," Int. J. Radiat. Oncol., Biol., Phys. **101**(3), 671–679 (2018).
12. J. M. Molkentine, T. N. Fujimoto, T. D. Horvath, *et al.*, "Enteral activation of WR-2721 mediates radioprotection and improved survival from lethal fractionated radiation," Sci. Rep. **9**(1), 1949 (2019).
13. T. N. Fujimoto, L. E. Colbert, Y. Huang, *et al.*, "Selective egln inhibition enables ablative radiotherapy and improves survival in unresectable pancreatic cancer," Cancer Res. **79**(9), 2327–2338 (2019).
14. S. H. Thorne and C. H. Contag, "Using in vivo bioluminescence imaging to shed light on cancer biology," Proc. IEEE **93**(4), 750–762 (2005).
15. K. O'Neill, S. K. Lyons, W. M. Gallagher, *et al.*, "Bioluminescent imaging: A critical tool in pre-clinical oncology research," J. Pathol. **220**(3), 317–327 (2010).
16. D. M. Close, T. T. Xu, G. S. Sayler, *et al.*, "In vivo bioluminescent imaging (BLI): Noninvasive visualization and interrogation of biological processes in living animals," Sensors **11**(1), 180–206 (2010).
17. R. Tuli, A. Surmak, J. Reyes, *et al.*, "Development of a novel preclinical pancreatic cancer research model: Bioluminescence image-guided focal irradiation and tumor monitoring of orthotopic xenografts," Transl. Oncol. **5**(2), 77–84 (2012).
18. S. Rapic, T. Samuel, P. E. Lindsay, *et al.*, "Assessing the accuracy of bioluminescence image-guided stereotactic body radiation therapy of orthotopic pancreatic tumors using a small animal irradiator," Radiat. Res. **197**(6), 1 (2022).
19. J. J. Yu, B. Zhang, I. I. Iordachita, *et al.*, "Systematic study of target localization for bioluminescence tomography guided radiation therapy," Med. Phys. **43**(5), 2619–2629 (2016).
20. B. Zhang, K. K.-H. Wang, J. J. Yu, *et al.*, "Bioluminescence tomography-guided radiation therapy for preclinical research," Int. J. Radiat. Oncol., Biol., Phys. **94**(5), 1144–1153 (2016).
21. B. Zhang, J. W. Wong, Iordachita, *et al.*, "Evaluation of on- and off-line bioluminescence tomography system for focal irradiation guidance," Radiat. Res. **186**(6), 592–601 (2016).
22. J. Shi, T. S. Udayakumar, Z. Wang, *et al.*, "Optical molecular imaging-guided radiation therapy part 1: Integrated x-ray and bioluminescence tomography," Med. Phys. **44**(9), 4786–4794 (2017).
23. J. Shi, T. S. Udayakumar, K. Xu, *et al.*, "Bioluminescence tomography guided small-animal radiation therapy and tumor response assessment," Int. J. Radiat. Oncol., Biol., Phys. **102**(4), 848–857 (2018).
24. Z. Deng, X. Xu, T. Garzon-Muvdi, *et al.*, "In vivo bioluminescence tomography center of mass-guided conformal irradiation," Int. J. Radiat. Oncol., Biol., Phys. **106**(3), 612–620 (2020).
25. X. Xu, Z. Deng, H. Dehghani, *et al.*, "Quantitative bioluminescence tomography-guided conformal irradiation for preclinical radiation research," Int. J. Radiat. Oncol., Biol., Phys. **111**(5), 1310–1321 (2021).
26. X. Xu, Z. Deng, D. Sforza, *et al.*, "Characterization of a commercial bioluminescence tomography-guided system for pre-clinical radiation research," Med. Phys. **50**(10), 6433–6453 (2023).
27. C. Kuo, O. Coquoz, T. L. Troy, *et al.*, "Three-dimensional reconstruction of in vivo bioluminescent sources based on multispectral imaging," J. Biomed. Opt. **12**(2), 024007 (2007).
28. H. Dehghani, S. C. Davis, S. D. Jiang, *et al.*, "Spectrally resolved bioluminescence optical tomography," Opt. Lett. **31**(3), 365–367 (2006).
29. A. D. Klose and T. Poschinger, "Excitation-resolved fluorescence tomography with simplified spherical harmonics equations," Phys. Med. Biol. **56**(5), 1443–1469 (2011).
30. M. A. Lewis, E. Richer, N. V. Slavine, *et al.*, "A multi-camera system for bioluminescence tomography in preclinical oncology research," Diagnostics **3**(3), 325–343 (2013).
31. H. Dehghani, J. A. Guggenheim, S. L. Taylor, *et al.*, "Quantitative bioluminescence tomography using spectral derivative data," Biomed. Opt. Express **9**(9), 4163–4174 (2018).
32. Z. Deng, X. Xu, I. Iordachita, *et al.*, "Mobile bioluminescence tomography-guided system for pre-clinical radiotherapy research," Biomed. Opt. Express **13**(9), 4970–4989 (2022).

Biomedical Optics EXPRESS

33. M. Schweiger, S. R. Arridge, M. Hiraoka, *et al.*, "The finite-element method for the propagation of light in scattering media - boundary and source conditions," Med. Phys. **22**(11), 1779–1792 (1995).
34. H. R. A. Basevi, K. M. Tichauer, F. Leblond, *et al.*, "Compressive sensing based reconstruction in bioluminescence tomography improves image resolution and robustness to noise," Biomed. Opt. Express **3**(9), 2131–2141 (2012).
35. A. D. Klose and N. Paragas, "Automated quantification of bioluminescence images," Nat. Commun. **9**(1), 4262 (2018).
36. D. R. Reed, A. A. Bachmanov, and M. G. Tordoff, "Forty mouse strain survey of body composition," Physiol. Behav. **91**(5), 593–600 (2007).
37. S. L. Jacques, "Optical properties of biological tissues: A review," Phys. Med. Biol. **58**(11), R37–R61 (2013).
38. J. Virostko, A. C. Powers, and E. D. Jansen, "Validation of luminescent source reconstruction using single-view spectrally resolved bioluminescence images," Appl. Opt. **46**(13), 2540–2547 (2007).
39. M. A. Naser, M. S. Patterson, and J. W. Wong, "Algorithm for localized adaptive diffuse optical tomography and its application in bioluminescence tomography," Phys. Med. Biol. **59**(8), 2089–2109 (2014).
40. A. Bentley, X. K. Xu, Z. J. Deng, *et al.*, "Simultaneous diffuse optical and bioluminescence tomography to improve source localization," in *European Conferences on Biomedical Optics - Diffuse Optical Spectroscopy and Imaging VIII, Proceedings of SPIE* (Spie-Int Soc Optical Engineering, 2021).
41. A. Bentley, X. Xu, Z. Deng, *et al.*, "Quantitative molecular bioluminescence tomography," J. Biomed. Opt. **27**(06), 066004 (2022).
42. R. Ali, S. Apte, M. Vilalta, *et al.*, "F-18-EF5 PET is predictive of response to fractionated radiotherapy in preclinical tumor models," PLoS One **10**(10), e0139425 (2015).
43. E. Reijmen, S. De Mey, W. De Mey, *et al.*, "Fractionated radiation severely reduces the number of CD8+ T cells and mature antigen presenting cells within lung tumors," Int. J. Radiat. Oncol., Biol., Phys. **111**(1), 272–283 (2021).
44. I. S. Juvkam, O. Zlygosteva, D. Arous, *et al.*, "A preclinical model to investigate normal tissue damage following fractionated radiotherapy to the head and neck," J. Radiat. Res. **64**(1), 44–52 (2023).
45. K. J. McKelvey, A. L. Hudson, H. Donaghy, *et al.*, "Differential effects of radiation fractionation regimens on glioblastoma," Radiat. Oncol. **17**(1), 17 (2022).